

## Article

# Characterization of Graphenic Carbon Produced by Pulsed Laser Ablation of Sacrificial Carbon Tapes

Igor V. Ershov <sup>1,\*</sup>, Anatoly A. Lavrentyev <sup>2</sup>, Natalia V. Prutsakova <sup>1</sup>, Olga M. Holodova <sup>1</sup>, Irina V. Mardasova <sup>1</sup>, Tatiana P. Zhdanova <sup>1</sup> and Alexey T. Kozakov <sup>3</sup>

<sup>1</sup> Department of Physics, Don State Technical University, 344000 Rostov-on-Don, Russia; shpilevay@mail.ru (N.V.P.); olga15@mail.ru (O.M.H.); irina.mardasowa@yandex.ru (I.V.M.); zhdanovatp@gmail.com (T.P.Z.)

<sup>2</sup> Department of Electrical Engineering and Electronics, Don State Technical University, 344000 Rostov-on-Don, Russia; alavrentyev@donstu.ru

<sup>3</sup> Research Institute of Physics, Southern Federal University, 344090 Rostov-on-Don, Russia; atkozakov@sfedu.ru

\* Correspondence: iershov@donstu.ru

**Abstract:** This paper reports on the pulsed laser deposition of nanocarbon films on metal and dielectric substrates, using high-purity sacrificial carbon tape as a carbon source on a neutral gas background. The films were characterized by X-ray diffraction (XRD), photoelectron (XPS) and Raman spectroscopy. The XRD and Raman structural analyses revealed that the synthesized films have a graphenic nanocrystalline turbostratic structure, with  $sp^2$  clusters about 15–18 nm in size, depending on the laser fluence. A significant decrease in the oxygen and hydrogen contents in the films, in comparison with the target material, was established using XPS, as well as a significant decrease in the  $sp^3$  carbon content. The deposited films were found to be similar to reduced graphene oxide (rGO) in composition, with a surprisingly low number of defects in the  $sp^2$ -matrix. The method proposed in the work may have good prospects of application in the production of energy storage and nonvolatile memory devices.

**Keywords:** graphenic carbon; reduced graphene oxide; Raman spectroscopy; XRD and XPS characterization; pulsed laser ablation



**Citation:** Ershov, I.V.; Lavrentyev, A.A.; Prutsakova, N.V.; Holodova, O.M.; Mardasova, I.V.; Zhdanova, T.P.; Kozakov, A.T. Characterization of Graphenic Carbon Produced by Pulsed Laser Ablation of Sacrificial Carbon Tapes. *Appl. Sci.* **2021**, *11*, 11972. <https://doi.org/10.3390/app112411972>

Academic Editors: Filippo Giannazzo and Ivan Shteplyuk

Received: 17 November 2021

Accepted: 14 December 2021

Published: 16 December 2021

**Publisher's Note:** MDPI stays neutral with regard to jurisdictional claims in published maps and institutional affiliations.



**Copyright:** © 2021 by the authors. Licensee MDPI, Basel, Switzerland. This article is an open access article distributed under the terms and conditions of the Creative Commons Attribution (CC BY) license (<https://creativecommons.org/licenses/by/4.0/>).

## 1. Introduction

Amorphous and crystalline  $sp^2$  carbon has attracted great interest in the fields of materials science and engineering, because of its unique physical, chemical and mechanical properties [1–3]. Graphenic quantum confined structures, such as graphene quantum dots (GQDs) and graphene oxide quantum dots (GOQDs), have shown promising applications in the fields of catalysis, optoelectronics, energy storage, and bio-imaging [4–7]. The attractive photoluminescent properties of GQDs place them amongst the new optical materials for advanced applications, such as light-emitting devices, optical sensing, and bio-imaging. GQDs exhibit a high quantum yield with excellent photostability, owing to the intrinsic band structure and physicochemical robustness, which is beneficial for optoelectronic applications [6]. Recently, much attention has been focused on the use of amorphous carbon for fast switching devices [8,9] and nonvolatile memory (NVM) applications [10,11]. Different switching mechanisms, from  $sp^2$ -dominated graphite-like amorphous carbon with low resistivity to the  $sp^3$ -dominated diamond-like form with high resistivity, have been reported [12]. It was shown that changing the  $sp^2/sp^3$  ratio can significantly influence the conduction behavior of carbon films [10].

Carbon-based layered and two-dimensional materials, including turbostratic carbon and multilayer graphene, are of great interest because of their high potential for electrochemical and biosensing applications [13]. These materials exhibit a large surface area,

which can be further modified by the generation of pores and the incorporation of dopants. Graphene-rich amorphous films also have prospective applications in surface modification, due to their chemical inertness, and excellent friction and wear performance [1,14], as well as their low internal stress and high conductivity. In contrast to pristine graphite and graphene, graphene-like carbon (GLC) and related materials, including reduced graphene oxide, contain lattice defects and residual oxygen-containing functional groups, which are beneficial for their capacitance and electron transfer kinetics. The reduction of graphene oxide (GO) has recently been considered as one of the promising methods for the large-scale production of graphene [15–17]. The main advantages of GO and related materials are: their excellent water dispersibility, inexpensive production, and tunability of physical and chemical properties by controlling the number of functional groups. Reduced graphene oxide is a conductive material of high potential importance in electronic applications, including optoelectronics [18], composite materials, sensors, and wearable technology [19]. Other promising applications of rGO include energy storage devices and nonvolatile resistive random access memory (RRAM) devices. Reduced graphene oxide and so-called graphene-like graphite (GLG) have been successfully used to create electrodes for supercapacitors and Li-ion batteries [13,16,20]. Additionally, rGO has been successfully applied in ITO/rGO/ITO transparent and flexible RRAM cells [21], with multilevel switching properties and relatively high endurance.

The common methods of GO reduction involve using electron beams, laser irradiation, heat, and chemical reduction. Recently, laser irradiation has been proposed as a promising tool for the reduction of GO [16,18,19,22]. The laser reduction of GO is based on the photochemical removal of oxygen functional groups from the GO surface, which is accompanied by laser ablation and molecular restructuring of the carbon lattice into the  $sp^2$ -conjugated graphene structure [22]. Laser reduction has many advantages over these methods. In addition to the spatial control and energy efficiency, the laser reduction process is much cleaner and less toxic than any chemical method, as it does not require chemical reactions in strong acids, or long-term washing procedures [16,19]. It is also important to note that laser processing can be easily adapted to lithography. In comparison with other physical and chemical methods of deposition, pulsed laser ablation is considered to be conceptually simple, rapid, and a versatile thin-film growth process. Pulsed laser ablation can be performed in either an ultra-high vacuum or in ambient gas, and allows for the deposition of any kind of carbon material, including carbon nanotubes, graphite- and diamond-like (DLC) carbon coatings [23–25], and even graphene films [26,27]. Recently, wavelength-modulated pulsed laser ablation in liquid (PLAL) was successfully applied for the selective and efficient production of GQDs and GOQDs [6]. PLD usually requires a graphite target, such as highly oriented pyrolytic graphite (HOPG) as a carbon source; however, in this work, we used sacrificial carbon tapes, which are commonly used in low-temperature co-fired ceramics technology (LTCC) [28] as a carbon source for laser ablation, to obtain  $sp^2$  nanocarbon with a reduced number of functional groups.

## 2. Materials and Methods

As a target material for laser ablation, we used the commercial carbon tape TCS-CARB-1 from the manufacturer C12 Advanced Technologies [29], which is typically composed of micro/nanocrystalline graphite-like carbon of high purity, dispersed in an organic vehicle.

Carbon films were prepared by PLD using 1064 nm IR Q-switched Nd:YAG laser with 40 ns pulse width. The use of 1064 nm wavelength was due to the fact that graphenic carbon with a significant oxygen content (including GO) demonstrates high absorptivity in the near- and mid-IR regions [16], so the irradiation of 1064 nm laser pulse should generate instantaneous and strong localized heating and burst apart the oxygen functional groups. On the other hand, the photon energy of 1064 nm irradiation is not sufficient for C=C bond photoionization, which should reduce the number of structural defects in the  $sp^2$  network in comparison with shorter wavelengths. We used nanosecond laser pulses in order to keep electronic subsystem in thermal equilibrium with lattice, which results in

more uniform heating [30]. The deposition was performed in specially designed inert chamber (Figure 1) on a He background at room temperature onto sapphire and silver substrates. Prior to the deposition, the substrates were ultrasonically cleaned in deionized water and isopropyl alcohol. The use of an inert gas was due to the need to remove the decomposition products of the organic vehicle from the deposition chamber. For this purpose, He was continuously pumped through the chamber at atmospheric pressure. Two different laser energies, namely,  $6 \text{ J/cm}^2$  (GLC/sapphire-1) and  $4 \text{ J/cm}^2$  (GLC/sapphire-2), were used for deposition on sapphire substrates. The laser fluences were chosen based on preliminary experiments and previous works [3,18,27]. The samples on conductive silver substrate (laser fluence— $4 \text{ J/cm}^2$ ) were used for the XPS measurements. During deposition, the substrate–target distance was fixed at 25 mm for all the samples. The laser beam, which focused on the spot of  $\sim 100 \mu\text{m}$ , using 20 cm focal length F-Theta lens, was continuously moved over the target surface at a speed of 3 mm/s using a scanning module with two galvanometers. The scanning speed was selected based on the thickness of the carbon tape. The laser spot was moved over the target in the spiral trajectory. The total ablated area on the carbon target was about 5 mm in diameter. We used a high pulse repetition rate of 500 Hz and a deposition time of 10 s for all samples.

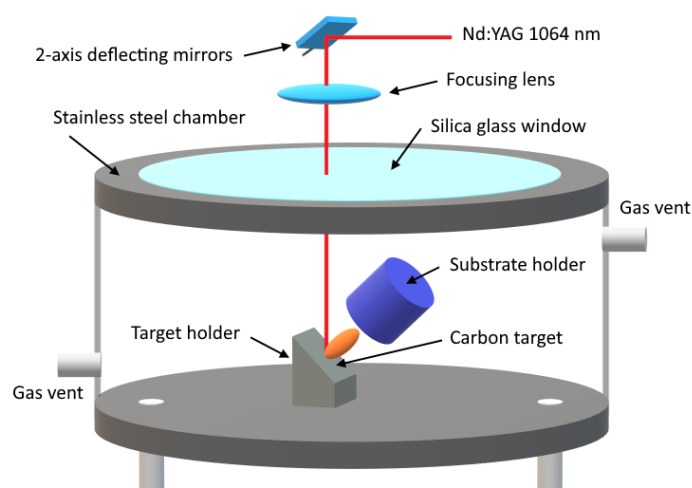


**Figure 1.** Schematic of the laser ablation process.

The XRD measurements were carried out using  $\text{Cu } K\alpha$  radiation (DRON-3 double-crystal diffractometer) in Bragg–Brentano focusing geometry. XPS was used to study the features of the chemical bonds on the surface layers of carbon films. XPS spectra were obtained with ESCALAB 250 spectrometer using monochromated  $\text{Al } K\alpha$  radiation (1486.6 eV). The energy resolution measured on the  $\text{Ag}3d_{5/2}$  line was 0.6 eV. Raman spectra were measured at room temperature with a Renishaw inVia Raman microspectrometer equipped with a 2.41 eV excitation energy  $\text{Ar}^+$  laser (514.5 nm). The spot size was  $\sim 4 \mu\text{m}$  focused with a  $50\times$  objective. The laser power was kept lower than 4 mW to avoid laser-induced heating and damage to the samples. The spectra were collected from the different points in both the central and edge regions of the films. No fundamental differences were observed between the spectra in each of the sample regions. The edge regions, however, demonstrated a significant photoluminescent background. For the same reason, it was not possible to obtain the Raman spectrum of the target carbon tape.

### 3. Results

The diffraction pattern of the target material (Figure 2) demonstrates the appearance of broadened 002 ( $2\theta = 25^\circ$ ) and 10 ( $2\theta = 43^\circ$ ) turbostratic carbon peaks, and is similar to the carbon black XRD pattern [31]. From peak position and FWHM evaluation, the crystallite sizes in the [001] and [100] directions were 1.6 nm and 3.1 nm, respectively [32]. The averaged interplanar distance between the graphene layers was  $\sim 3.7 \text{ \AA}$ .

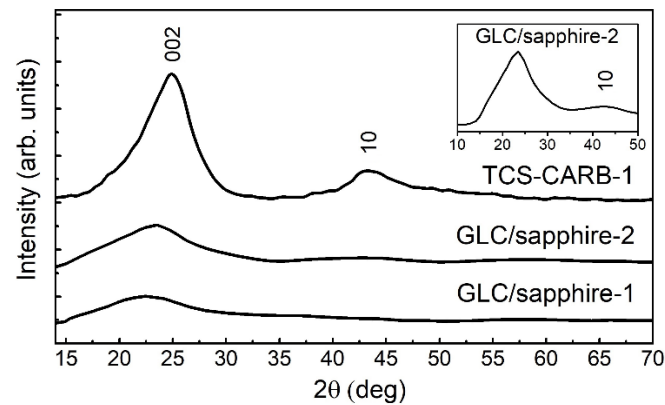


**Figure 2.** XRD patterns of the target material and carbon films on sapphire substrate.

The diffraction spectra of the carbon films deposited on sapphire (Figure 2) exhibit less intense, broad 002 peaks, slightly shifted to lower angles in comparison with the corresponding target peak. The peak shift is due to the increase in interlayer spacing, by about 0.1 Å. Additionally, a weakly resolved bump at  $2\theta \approx 43^\circ$  can be observed for the GLC/sapphire-2 sample (inset in Figure 2), which lies in the region of 10 reflections. The resulting diffractograms are characteristic of a turbostratic structure [31,33,34], and are similar to the reduced graphene oxide XRD pattern [35].

Figure 3a shows the survey XPS spectrum of the TCS-CARB-1 target material. This spectrum only features carbon and oxygen peaks. Figure 3b demonstrates the high-resolution C1s core-level XPS spectrum of the target. This spectrum was deconvoluted into five different chemically shifted components. The XPS data are shown in Table 1. Peak A (284.3 eV) is related to  $sp^2$ -bonded carbon atoms with perfect graphene lattices (C=C bond) [36]. We attribute peak B (285.6 eV) to the carbon being partially  $sp^3$  bonded [37], and to the presence of  $sp^3$ -hybridized C–H bonds [32]. The peaks C, D and E correspond to the following oxygen-containing groups: epoxide (C–O–C) [35,38,39] and hydroxyl groups ( $\sim 287$  eV), C=O carbonyl groups (288.5 eV) [40,41], and carboxyl O=C–OH groups (289.9 eV) [42].

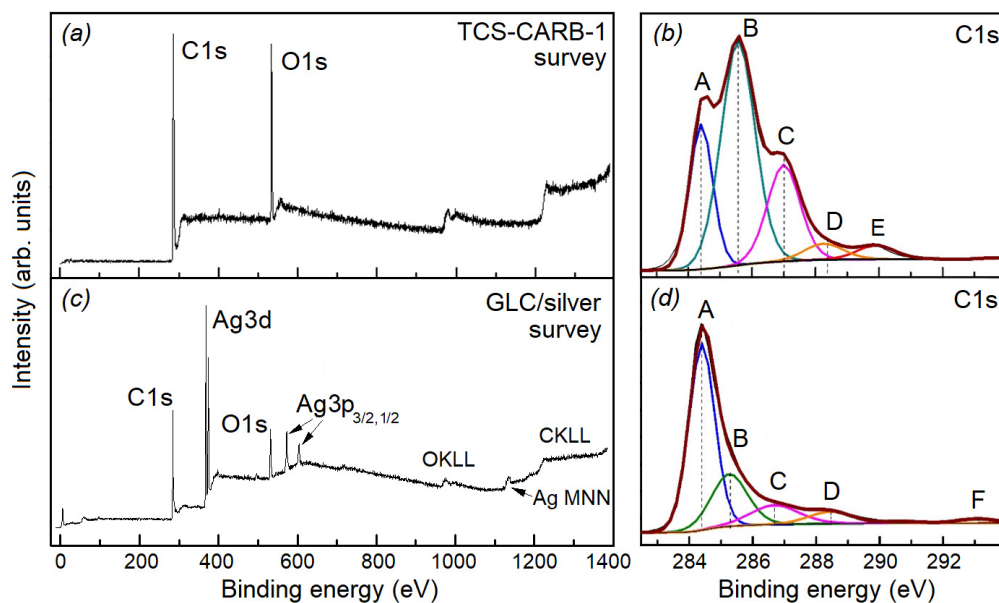


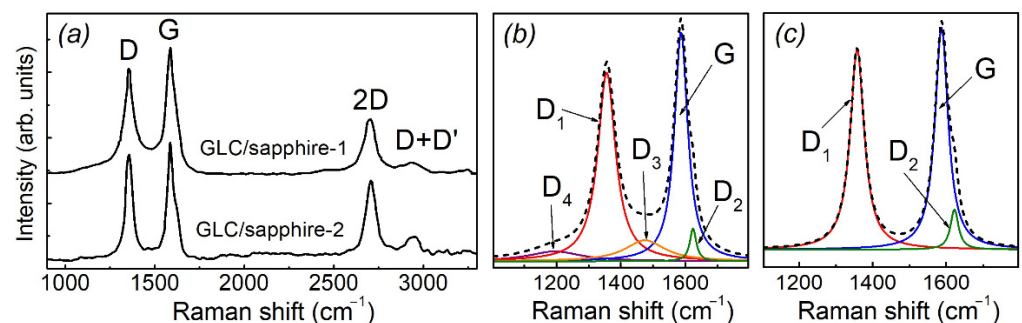
**Figure 3.** XPS spectra of the target material and carbon film, deposited on silver. Survey (a,c) and high-resolution C1s spectra (b,d).

**Table 1.** The percentage of carbon bonds in the target material and in the carbon film deposited on silver.

C1s	A	B	C	D	E	sp <sup>2</sup> /sp <sup>3</sup>
	C=C (sp <sup>2</sup> )	C-C (sp <sup>3</sup> ), C-COOH	C-O-C, C-OH	C=O	O=C-OH	
TCS-CARB-1	21% (284.3 eV)	46.4% (285.6 eV)	22.2% (287 eV)	5.2% (288.3 eV)	5.2% (289.9 eV)	0.47
GLC/Ag	59.3% (284.4 eV)	23.6% (285.3 eV)	12.4% (286.7 eV)	4.7% (288.5 eV)	-	2.51

Figure 3c demonstrates the survey XPS spectrum of the GLC film deposited on silver substrate. The spectrum features carbon, oxygen and silver peaks. The high-resolution C1s XPS spectrum of the nanocarbon film is presented in Figure 3d. The C1s spectrum features similar A, B, C and D peaks, with modified positions and intensities. Peak A (284.4 eV), with increased intensity, is still related to sp<sup>2</sup>-bonded graphenic carbon. In contrast, peak B (285.3 eV) shifted to lower energy, and its intensity decreased significantly compared to peak A. The latter can be explained by a significant decrease in the content of organic vehicle, and, accordingly, in the content of C–H bonds. The ratio of the integral intensities of A/B can be used to estimate the sp<sup>2</sup>/sp<sup>3</sup> fraction in the material (Table 1) [43]. Compared to the target material, peak C is shifted towards lower binding energies and has a much lower intensity, which may indicate the loss of oxygen from epoxy and hydroxyl groups as a result of ablation, and a decrease in the fraction of epoxy groups relative to hydroxyl groups. The component D only slightly decreased in intensity. It should be noted that the F component appears in the spectrum of the film, which is interpreted as a  $\pi \rightarrow \pi^*$  shake-up satellite [44]. The latter indicates an increase in the fraction of sp<sup>2</sup> carbon.

Figure 4a shows the Raman spectra of the two carbon films, deposited on sapphire at different laser fluxes. The spectra demonstrate three intense bands, namely, G (~1586 cm<sup>-1</sup>), D (~1357 cm<sup>-1</sup>), and 2D (~2700 cm<sup>-1</sup>), which are characteristic of all graphenic carbons, including amorphous carbon [45]. The G band is a Raman-active E<sub>2g</sub> optical mode at the center of the Brillouin zone, and it indicates the presence of sp<sup>2</sup> carbon networks [45–47]. The D band is a defect-induced breathing A<sub>1g</sub> mode of six-member carbon rings. It originates from TO phonons near the BZ edge, and is active by double resonance [47,48]. The 2D band corresponds to the overtone of the D band. It originates from two-phonon scattering, and no defects are required for its activation [47,48]. Both D and 2D bands are due to the double resonance.

**Figure 4.** Raman spectra of carbon films, deposited on sapphire substrates (a), and first-order fitted spectra of the samples GLC/sapphire-1 (b) and GLC/sapphire-2 (c).

The Raman spectra also feature the peak D + D' (~2940 cm<sup>-1</sup>), which is a product of the two-phonon scattering process in the presence of defects [48]. Figure 4b shows the first-order region of the Raman spectrum of the GLC/sapphire-1 sample with Lorentzian fitting. The fitted spectrum includes the following five components: G, D<sub>1</sub>(D), D<sub>2</sub>(D'), D<sub>3</sub>, and D<sub>4</sub>. The D' (~1620 cm<sup>-1</sup>) is a defect-activated peak induced by a double-resonance

intra-valley process [44]. The assignment of the bands  $D_3$  and  $D_4$  is not obvious. The  $D_3$  band is commonly assigned to the presence of amorphous phases, connected to the polyaromatic planes through carbon  $sp^3$  bonds and out-plane defects [2,31,47], while the  $D_4$  band is attributed to hydrocarbons, adsorbed on the basal planes of graphenic layers [31,49]. The experimental data [31] show that the  $D_3$  band decreases to zero at a temperature above 1500 °C. It was also shown [31] that the  $D_4$  band disappears with heat treatment above 1200 °C. The first-order spectrum of the GLC/sapphire-2 sample (Figure 4c) was fitted using only the following three Lorentzian components: G, D, and D'.

#### 4. Discussion

The ratio of the D and G band intensities,  $I_D/I_G$ , is widely used for the quantitative evaluation of defects in graphitic materials [47,50,51]. For the given excitation laser wavelength  $\lambda_l$ , the following expression can be used to evaluate the  $sp^2$  cluster size  $L_a$  [51]:

$$L_a(\text{nm}) = 2.4 \cdot 10^{-10} \lambda_l^4 (I_D/I_G)^{-1} \quad (1)$$

From the  $I_D/I_G$  ratio, and the peak's position (Table 2) and shape, we can conclude that the films deposited on sapphire substrates correspond to the first or the second stage of disorder, according to the amorphization trajectory of Ferrari and Robertson [45,52]. The increase in structural disorder causes broadening of the D and G bands. The combination of the  $I_D/I_G$  ratio and full width at half maximum (FWHM) of the G band allows us to distinguish between stages 1 and 2 [48,53]. The positions of the G line in the spectra are upshifted by 6  $\text{cm}^{-1}$  and 5  $\text{cm}^{-1}$  for the GLC/sapphire-1 and GLC/sapphire-2 samples, respectively. We used the FWHM of the G band to evaluate the minimal  $sp^2$  cluster size in the samples, according to [53]. The evaluated minimal size was in the range of 6–10 nm. This allowed us to conclude that the samples correspond to the first stage of amorphization, for which Equation (1) is valid. The characteristic sizes of the graphenic clusters were found to be 15.3 nm and 17.7 nm for the GLC/sapphire-1 and GLC/sapphire-2 samples, respectively. These features in the Raman spectra allow us to conclude that the GLC/sapphire-1 film has a higher degree of structural disorder in comparison with the GLC/sapphire-2 sample. It can also be concluded that the deposited carbon films are similar to nanocrystalline graphite or disordered multilayer graphene in the degree of in-plane structural ordering.

**Table 2.** Positions (Pos.) of the most intense Raman peaks, full width at half maximum (FWHM), integral intensities ratio ( $I_D/I_G$ ) of the D and G peaks, and  $sp^2$  cluster size estimation ( $L_a$ ).

	Pos., $\text{cm}^{-1}$				FWHM, $\text{cm}^{-1}$			$I_D/I_G$	$L_a$ , nm
	D	G	2D	D'	D	G	2D		
GLC/sapphire-1	1356	1587	2701	1623	67	50	76	1.11	15.3
GLC/sapphire-2	1358	1586	2707	1621	45	43	63	0.96	17.7

The 2D Raman band of the graphite-like materials is very sensitive to the stacking order of the graphene layers along the [001] direction [47]. It was shown that the 2D bands in our second-order Raman spectra can be fitted using only one Lorentzian function, centered at 2701 and 2707  $\text{cm}^{-1}$  for the GLC/sapphire-1 and GLC/sapphire-2 samples, respectively. This indicates that the interaction between the graphenic planes is weak enough that there is no splitting in the  $\pi$ -electron dispersion energies [53,54], which is typical of the turbostratic structure of disordered multilayer graphene and reduced graphene oxide [26,27,31,33,34,54,55]. We also estimated the  $sp^2$  cluster size based on the FWHM of the 2D bands using the experimental data from the work [55]. The values 22 and 20 nm were obtained for the GLC/sapphire-1 and GLC/sapphire-2 samples, respectively, which is in good agreement with the previous estimations.

## 5. Conclusions

In this paper, we proposed a scalable method for the fabrication of graphenic carbon with a relatively low number of defects in the  $sp^2$  matrix, using pulsed laser ablation in an inert gas atmosphere. The use of an inert atmosphere instead of a vacuum significantly reduces the fabrication costs. The XPS data showed that the deposited films only contain carbon and oxygen in functional groups that are characteristic of reduced graphene oxide. The number of oxygen-containing groups significantly decreased as a result of laser exposure, and the fraction of  $sp^2$  carbon increased five times in comparison with the target material. Taking into account the XPS and Raman scattering data, we can conclude that the fabricated graphenic carbon is similar to reduced graphene oxide, with the  $sp^2$  clusters being about 15–18 nm in size. The XRD and Raman data also indicate the lack of ordering between the  $sp^2$  layers in the nanocarbon films. The latter may result in a significant increase in the effective surface area, which is beneficial for energy storage devices. The method proposed in this work, for the production of graphenic nanocarbon on dielectric substrates, may have good prospects for the manufacturing of transparent and flexible RRAM carbon-based cells.

**Author Contributions:** Conceptualization, I.V.E. and A.A.L.; Data curation, A.A.L. and N.V.P.; Formal analysis, A.A.L.; Investigation, N.V.P., I.V.M. and A.T.K.; Methodology, I.V.E. and A.A.L.; Project administration, A.A.L.; Resources, I.V.E.; Software, O.M.H. and T.P.Z.; Supervision, I.V.E.; Validation, N.V.P. and I.V.M.; Visualization, O.M.H.; Writing—original draft, I.V.E.; Writing—review & editing, A.A.L. All authors have read and agreed to the published version of the manuscript.

**Funding:** This research received no external funding.

**Institutional Review Board Statement:** Not applicable.

**Informed Consent Statement:** Not applicable.

**Data Availability Statement:** The data presented in this study are available on request from the corresponding author.

**Acknowledgments:** The authors are sincerely grateful to Avramenko M.V. (Nanotechnology department of the Southern Federal University) for carrying out experiments on Raman scattering.

**Conflicts of Interest:** The authors declare no conflict of interest. The funders had no role in the design of the study; in the collection, analyses, or interpretation of data; in the writing of the manuscript, or in the decision to publish the results.

## References

1. Huang, M.; Zhang, X.; Keb, P.; Wang, A. Graphite-like carbon films by high power impulse magnetron sputtering. *Appl. Surf. Sci.* **2013**, *283*, 321–326. [[CrossRef](#)]
2. Greco, C.; Cosentino, U.; Pitea, D.; Moro, G.; Santangelo, S.; Patane, S.; D'Arienzo, M.; Fiore, M.; Morazzoni, F.; Ruffo, R. Role of the carbon defects in the catalytic oxygen reduction by graphite nanoparticles: A spectromagnetic, electrochemical and computational integrated approach. *Phys. Chem. Chem. Phys.* **2019**, *21*, 6021–6032. [[CrossRef](#)] [[PubMed](#)]
3. Bleu, Y.; Bourquard, F.; Tite, T.; Loir, A.-S.; Maddi, C.; Donnet, C.; Garrelie, F. Review of Graphene Growth from a Solid Carbon Source by Pulsed Laser Deposition (PLD). *Front. Chem.* **2018**, *6*, 572–590. [[CrossRef](#)]
4. Abbas, A.; Mariana, L.T.; Phan, A.N. Biomass-waste derived graphene quantum dots and their applications. *Carbon* **2018**, *140*, 77–99. [[CrossRef](#)]
5. Jang, M.-H.; Yang, H.; Chang, Y.H.; Park, H.-C.; Park, H.; Cho, H.H.; Kim, B.J.; Kim, Y.-H.; Cho, Y.-H. Selective engineering of oxygen-containing functional groups using the alkyl ligand oleylamine for revealing the luminescence mechanism of graphene oxide quantum dot. *Nanoscale* **2017**, *9*, 18635. [[CrossRef](#)]
6. Kang, S.; Ryu, J.H.; Lee, B.; Jung, K.H.; Shim, K.B.; Han, H.; Kim, K.M. Laser wavelength modulated pulsed laser ablation for selective and efficient production of graphene quantum dots. *RSC Adv.* **2019**, *9*, 1365. [[CrossRef](#)]
7. Lyu, B.; Li, H.-J.; Xue, F.; Sai, L.; Gui, B.; Qian, D.; Wang, X.; Yang, J. Facile, gram-scale and eco-friendly synthesis of multicolor graphene quantum dots by thermal-driven advanced oxidation process. *Chem. Eng. J.* **2020**, *388*, 124285. [[CrossRef](#)]
8. Bhattacharyya, S.; Henley, S.J.; Mendoza, E.; Gomez-Rojas, L.; Allam, J.; Silva, S.R.P. Resonant tunnelling and fast switching in amorphous-carbon quantum-well structures. *Nat. Mater.* **2006**, *5*, 19–21. [[CrossRef](#)]
9. Tsanga, W.M.; Henley, S.J.; Stolojan, V.; Silva, S.R.P. Negative differential conductance observed in electron field emission from band gap modulated amorphous-carbon nanolayers. *Appl. Phys. Lett.* **2006**, *89*, 193103. [[CrossRef](#)]

10. Sebastian, A.; Pauza, A.; Rossel, C.; Shelby, R.M.; Rodríguez, A.F.; Pozidis, H.; Eleftheriou, E. Resistance switching at the nanometre scale in amorphous carbon. *New J. Phys.* **2011**, *13*, 013020. [CrossRef]
11. Santini, C.A.; Sebastian, A.; Marchiori, C.; Jonnalagadda, V.P.; Dellmann, L.; Koelmans, W.W.; Rossell, M.D.; Rossel, C.P.; Eleftheriou, E. Oxygenated amorphous carbon for resistive memory applications. *Nat. Commun.* **2015**, *6*, 8600. [CrossRef]
12. Hui, F.; Grustan-Gutierrez, E.; Long, S.; Liu, Q.; Ott, A.K.; Ferrari, A.C.; Lanza, M. Graphene and Related Materials for Resistive Random Access Memories. *Adv. Electron. Mater.* **2017**, *3*, 1600195. [CrossRef]
13. Cheng, Q.; Okamoto, Y.; Tamura, N.; Tsuji, M.; Maruyama, S.; Matsuo, Y. Graphene-Like-Graphite as Fast-Chargeable and High-Capacity Anode Materials for Lithium Ion Batteries. *Sci. Rep.* **2017**, *7*, 14782. [CrossRef]
14. Rybachuk, M.; Bell, J.M. The effect of sp<sup>2</sup> fraction and bonding disorder on micro-mechanical and electronic properties of aC:H films. *Thin Solid Films* **2007**, *515*, 7855–7860. [CrossRef]
15. Zhan, D.; Ni, Z.; Chen, W.; Sun, L.; Luo, Z.; Lai, L.; Yu, T.; Wee, A.T.S.; Shen, Z. Electronic structure of graphite oxide and thermally reduced graphite oxide. *Carbon* **2011**, *49*, 1362–1366. [CrossRef]
16. Bhattacharjya, D.; Kim, C.-H.; Kim, J.-H.; You, I.-K.; In, J.B.; Lee, S.-M. Fast and controllable reduction of graphene oxide by low-cost CO<sub>2</sub> laser for supercapacitor application. *Appl. Surf. Sci.* **2018**, *462*, 353–361. [CrossRef]
17. Azizighannad, S.; Mitra, S. Stepwise Reduction of Graphene Oxide (GO) and Its Effects on Chemical and Colloidal Properties. *Sci. Rep.* **2018**, *8*, 10083. [CrossRef] [PubMed]
18. Evlashin, S.; Dyakonov, P.; Khmel'nitsky, R.; Dagesyan, S.; Klokov, A.; Sharkov, A.; Timashev, P.; Minaeva, S.; Maslakov, K.; Svyakhovskiy, S.; et al. Controllable Laser Reduction of Graphene Oxide Films for Photoelectronic Applications. *ACS Appl. Mater. Interfaces* **2016**, *8*, 28880–28887. [CrossRef]
19. Rodríguez, R.D.; Khalelov, A.; Postnikov, P.S.; Lipovka, A.; Dorozhko, E.; Amin, I.; Murastov, G.V.; Chen, J.-J.; Sheng, W.; Trusova, M.E.; et al. Beyond graphene oxide: Laser engineering functionalized graphene for flexible electronics. *Mater. Horiz.* **2020**, *7*, 1030–1041. [CrossRef]
20. Foo, C.Y.; Sumboja, A.; Tan, D.J.H.; Wang, J.; Lee, P.S. Flexible and highly scalable V<sub>2</sub>O<sub>5</sub>-rGO electrodes in an organic electrolyte for supercapacitor devices. *Adv. Energy Mater.* **2014**, *4*, 1400236. [CrossRef]
21. Kim, H.-D.; Yun, M.J.; Lee, J.H.; Kim, K.H.; Kim, T.G. Transparent multi-level resistive switching phenomena observed in ITO/RGO/ITO memory cells by the sol-gel dip-coating method. *Sci. Rep.* **2014**, *4*, 4614. [CrossRef]
22. Zhao, Y.; Han, Q.; Cheng, Z.; Jiang, L.; Qu, L. Integrated graphene systems by laser irradiation for advanced devices. *Nano Today* **2017**, *12*, 14–30. [CrossRef]
23. Marquardt, C.L.; Williams, R.T.; Nagel, D.J. Deposition of amorphous carbon films from laser-produced plasmas. *Mat. Res. Soc.* **1985**, *38*, 325–335. [CrossRef]
24. Sikora, A.; Garrelie, F.; Donnet, C.; Loir, A.S.; Fontaine, J.; Sanchez-Lopez, J.C.; Rojas, T.C. Structure of diamondlike carbon films deposited by femtosecond and nanosecond pulsed laser ablation. *J. Appl. Phys.* **2010**, *108*, 113516. [CrossRef]
25. Acharya, K.P.; Khatri, H.; Marsillac, S.; Ullrich, B.; Anzenbacher, P.; Zamkov, M. Pulsed laser deposition of graphite counter electrodes for dye-sensitized solar cells. *Appl. Phys. Lett.* **2010**, *97*, 201108. [CrossRef]
26. Kumar, I.; Khare, A. Multi- and few-layer graphene on insulating substrate via pulsed laser deposition technique. *Appl. Surf. Sci.* **2014**, *317*, 1004–1009. [CrossRef]
27. Xu, S.C.; Man, B.Y.; Jiang, S.; Liu, A.H.; Hu, G.D.; Chen, C.S.; Liu, M.; Yang, C.; Feng, D.J.; Zhang, C. Direct synthesis of graphene on any nonmetallic substrate based on KrF laser ablation of ordered pyrolytic graphite. *Laser Phys. Lett.* **2014**, *11*, 096001. [CrossRef]
28. Birol, H.; Maeder, T.; Ryser, P. Application of graphite-based sacrificial layers for fabrication of LTCC (low temperature co-fired ceramic) membranes and micro-channels. *J. Micromech. Microeng.* **2007**, *17*, 50–60. [CrossRef]
29. C12 Advanced Technologies. Available online: <https://c12materials.com/services/fugitive-tapes/> (accessed on 1 November 2021).
30. Dumitru, G.; Romano, V.; Weber, H.P.; Pimenov, S.; Kononenko, T.; Sentis, M.; Hermann, J.; Bruneau, S. Femtosecond laser ablation of diamond-like carbon films. *Appl. Surf. Sci.* **2004**, *222*, 226–233. [CrossRef]
31. Pawlyta, M.; Rouzaud, J.-N.; Duber, S. Raman microspectroscopy characterization of carbon blacks: Spectral analysis and structural information. *Carbon* **2015**, *84*, 479–490. [CrossRef]
32. Cuesta, A.; Dhamelincourt, P.; Laureyns, J.; Martínez-Alonso, A.; Tascon, J.M.D. Comparative performance of X-ray diffraction and Raman microprobe techniques for the study of carbon materials. *J. Mater. Chem.* **1998**, *8*, 2875–2879. [CrossRef]
33. Sazali, N.E.S.; Deraman, M.; Omar, R.; Othman, M.A.R.; Suleman, M.; Shamsudin, S.A.; Tajuddin, N.S.M.; Hanappi, M.F.Y.M.; Hamdan, E.; Nor, N.S.M.; et al. Preparation and structural characterization of turbostratic-carbon/graphene derived from amylose film. *AIP Conf. Proc.* **2016**, *1784*, 040009. [CrossRef]
34. Navalon, S.; Herance, J.R.; Alvaro, M.; Garcia, H. General aspects in the use of graphenes in catalysis. *Mater. Horiz.* **2018**, *5*, 363–378. [CrossRef]
35. Rabchinskii, M.K.; Dideikin, A.T.; Kirilenko, D.A.; Baidakova, M.V.; Shnitov, V.V.; Roth, F.; Konyakhin, S.V.; Besedina, N.A.; Pavlov, S.I.; Kuricyn, R.A.; et al. Facile reduction of graphene oxide suspensions and films using glass wafers. *Sci. Rep.* **2018**, *8*, 14154. [CrossRef]
36. Xu, T.; Yang, S.; Lu, J.; Xue, Q.; Li, J.; Guo, W.; Sun, Y. Characterization of nanocrystalline diamond films implanted with nitrogen ions. *Diam. Relat. Mater.* **2001**, *10*, 1441–1447. [CrossRef]

37. Haerle, R.; Riedo, E.; Pasquarello, A.; Baldereschi, A.  $sp^2/sp^3$  hybridization ratio in amorphous carbon from C 1s core-level shifts: X-ray photoelectron spectroscopy and first-principles calculation. *Phys. Rev. B* **2001**, *65*, 045101. [[CrossRef](#)]
38. Chen, L.; Xu, Z.; Li, J.; Zhou, B.; Shan, M.; Li, Y.; Liu, L.; Li, B.; Niu, J. Modifying graphite oxide nanostructures in various media by high-energy irradiation. *RSC Adv.* **2014**, *4*, 1025–1031. [[CrossRef](#)]
39. Rani, J.R.; Lim, J.; Oh, J.; Kim, D.; Lee, D.; Kim, J.W.; Shin, H.S.; Kim, J.H.; Jun, S.C. Substrate and buffer layer effect on the structural and optical properties of graphene oxide thin films. *RSC Adv.* **2013**, *3*, 5926–5936. [[CrossRef](#)]
40. Watts, J.F.; Wilstenholme, J. *An Introduction to Surface Analysis by XPS and AES*; John Wiley & Sons, Ltd.: Chichester, UK, 2003. [[CrossRef](#)]
41. Briggs, E.D.; Seach, M.P. *Practical Surface Analysis by Auger and X-ray Photoelectron Spectroscopy*; John Wiley & Sons, Ltd.: Chichester, UK, 1983.
42. Ganguly, A.; Sharma, S.; Papakonstantinou, P.; Hamilton, J. Probing the thermal deoxygenation of graphene oxide using high-resolution in situ X-ray-based spectroscopies. *J. Phys. Chem. C* **2011**, *115*, 17009–17019. [[CrossRef](#)]
43. Kumar, N.; Ramadoss, R.; Kozakov, A.T.; Jothiramalingam, S.K.; Dash, S.; Tyagi, A.K.; Tai, N.H.; Lin, I.-N. Humidity-dependent friction mechanism in an ultrananocrystalline diamond film. *J. Phys. D Appl. Phys.* **2013**, *46*, 275501. [[CrossRef](#)]
44. Piecuch, P.; Maruani, J.; Delgado-Barrio, G.; Wilson, S. *Advances in the Theory of Atomic and Molecular Systems*; Springer: Dordrecht, The Netherlands; Berlin/Heidelberg, Germany; London, UK; New York, NY, USA, 2009. [[CrossRef](#)]
45. Ferrari, A.C.; Robertson, J. Interpretation of Raman spectra of disordered and amorphous carbon. *Phys. Rev. B* **2000**, *61*, 14095–14107. [[CrossRef](#)]
46. Ferrari, A.C. Raman spectroscopy of graphene and graphite: Disorder, electron-phonon coupling, doping and nonadiabatic effects. *Sol. State Comm.* **2007**, *143*, 47–57. [[CrossRef](#)]
47. Pimenta, M.A.; Dresselhaus, G.; Dresselhaus, M.S.; Cancado, L.G.; Jorio, A.; Saito, R. Studying disorder in graphite-based systems by Raman spectroscopy. *Phys. Chem. Chem. Phys.* **2007**, *9*, 1276–1296. [[CrossRef](#)]
48. Ferrari, A.C.; Basko, D.M. Raman spectroscopy as a versatile tool for studying the properties of graphene. *Nat. Nanotech.* **2013**, *8*, 235–246. [[CrossRef](#)]
49. Sadezky, A.; Muckenhuber, H.; Grothe, H.; Niessner, R.; Poschl, U. Raman microspectroscopy of soot and related carbonaceous materials: Spectral analysis and structural information. *Carbon* **2005**, *43*, 1731–1742. [[CrossRef](#)]
50. Tuinstra, F.; Koenig, J.L. Raman spectrum of graphite. *J. Chem. Phys.* **1970**, *53*, 1126–1130. [[CrossRef](#)]
51. Cancado, L.G.; Takai, K.; Enoki, T.; Endo, M. General equation for the determination of the crystallite size  $L_a$  of nanographite by Raman spectroscopy. *Appl. Phys. Lett.* **2006**, *88*, 163106. [[CrossRef](#)]
52. Ferrari, A.C.; Robertson, J. Resonant Raman spectroscopy of disordered, amorphous, and diamondlike carbon. *Phys. Rev. B* **2001**, *64*, 075414. [[CrossRef](#)]
53. Ferrari, A.C.; Rodil, S.E.; Robertson, J. Interpretation of infrared and Raman spectra of amorphous carbon nitrides. *Phys. Rev. B* **2003**, *67*, 155306. [[CrossRef](#)]
54. Wei, C.; Negishi, R.; Ogawa, Y.; Akabori, M.; Taniyasu, Y.; Kobayashi, Y. Turbostratic multilayer graphene synthesis on CVD graphene template toward improving electrical performance. *Jpn. J. Appl. Phys.* **2019**, *58*, SIIB04. [[CrossRef](#)]
55. Cancado, L.G.; Jorio, A.; Pimenta, M.A. Measuring the absolute Raman cross section of nanographites as a function of laser energy and crystallite size. *Phys. Rev. B* **2007**, *76*, 064304. [[CrossRef](#)]